PAPER

A flexible and highly sensitive pressure sensor based on three-dimensional electrospun carbon nanofibers†

Chuan Cai, [ID] [a] He Gong,[a] Weiping Li,[b] Feng Gao,[c] Qiushi Jiang,[b] Zhiqiang Cheng, [ID] *[b] Zhaolian Han[b] and Shijun Li*[a]

High-performance flexible pressure sensors with high sensitivity are important components of the systems for healthcare monitoring, human–machine interaction, and electronic skin. Herein, a flexible and highly sensitive pressure sensor composed of ferrosoferric oxide (Fe_3O_4)/carbon nanofibers (FeOCN) was fabricated using three-dimensional electrospinning and further heat treatment methods. The obtained pressure sensor demonstrates a wide working range (0–4.9 kPa) and a high sensitivity of 0.545 kPa^{-1} as well as an ultralow detection limit of 6 Pa. Additionally, the pressure sensor exhibits a rapid response time, good stability, high hydrophobicity, and excellent flexibility. These merits endow the pressure sensor with the ability to precisely detect wrist pulse, phonation, breathing, and finger bending in real-time. Therefore, the FeOCN pressure sensor presents a promising application in real-time healthcare monitoring.

1. Introduction

Flexible and highly sensitive pressure sensors have attracted tremendous attention in recent years[1] due to their various promising applications, including healthcare monitoring,[2] human–machine interaction, and electronic skin.[3,4] To date, a great number of pressure sensors have been designed and the transduction mechanisms can be mainly classified as four types: piezoresistivity,[4] capacitance,[5] piezoelectricity,[6] and triboelectricity.[7] Particularly, piezoresistive pressure sensors are commonly researched for their demonstrated great merits such as uncomplicated device structure, simple signal acquisition, good stability, and large working range.[1,8,9] By translating mechanical deformations into electrical resistance signals of piezoresistive materials, piezoresistive pressure sensors can detect various transient or static mechanical stimuli.[1,10]

Flexible piezoresistive pressure sensors are generally prepared from two key components.[11] One is a conductive material and the other is a flexible elastomeric matrix. To date, many studies have chosen expensive conductive materials for flexible piezoresistive pressure sensors, such as carbon nanotubes,[12] Ag nanowires (AgNWs),[13] Au nanowires (AuNWs),[14]

graphene[15] and reduced graphene,[16] in which AgNWs and AuNWs are relatively expensive as well as based on non-abundant metal. Various complicated process methods, including chemical vapor deposition (CVD) followed by etching,[17] freeze-drying plus carbonization,[18,19] and template combined with *in situ* polymerization process[20] have been used to construct various sophisticated microstructures for piezoresistive pressure sensors. For instance, Ma Yuxiao *et al.* prepared graphene–amorphous carbon hierarchical foam (G–ACHF) by chemical vapor deposition (CVD), followed by etching process.[17] Hu Yijie *et al.* reported a carbon aerogel piezoresistive pressure sensor with directional freeze-drying and carbonization process.[19] Wan Yuqin *et al.* fabricated a porous conductive polyurethane (PU) sponge force sensor based on *in situ* polymerization of pyrrole inside the porous polyurethane elastomer, in which porous polyurethane elastomer was prepared by a sugar-templated.[20] However, the fabrication of these aforementioned three-dimensional piezoresistive pressure sensors is often complicated and not easy to implement.

Electrospinning is a simple, effective, and cheap technique for manufacturing ultrafine continuous fibers with diameters from micrometer to nanometer scale.[21,22] Meanwhile, electrospinning technology is often used to prepare two-dimensional (2D) nanofibers, but it also holds great promise as a robust method for preparing 3D nanofibers.[23,24] Compared with the 2D nanofibers, the 3D nanofibers tend to be formed with a significant increase in thickness and porosity. And 3D electrospun nanofibers are widely applied in tissue engineering.[21] There are few reports on the use of 3D electrospun nanofibers for flexible pressure sensors,[2,25] especially the use of electrospun 3D

[a]College of Information Technology, Jilin Agricultural University, 2888 Xincheng Street, Changchun 130118, China. E-mail: lsj0883@sina.com

[b]College of Resources and Environment, Jilin Agriculture University, 2888 Xincheng Street, Changchun, 130118, China. E-mail: czq5974@163.com

[c]College of Plant Protection, Jilin Agriculture University, Changchun 130118, China

carbonized nanofibers for pressure sensing.[25] In addition, compared with various sophisticated microstructure designs for flexible pressure sensors, such as micropyramid structure,[26] porous structure,[27] nano-architected multilevel ridges,[28] and micropillar structure,[29] the interweaved 3D nanofibers network structure can be directly obtained by simple electrospinning.

In this paper, we reported a flexible and highly sensitive pressure sensor composed of ferrosoferric oxide (Fe_3O_4)/carbon nanofibers (FeOCN) was fabricated using three-dimensional electrospinning and further heat treatment methods. Our method for producing flexible 3D carbon nanofibers has great advantages because the precursor solution can simultaneous building of a 3D nanofibers network structure and enable the FeOCN to overcome the intrinsic brittleness of PAN-based carbon nanofibers (CNFs).[30] Owing to the flexible 3D carbon nanofibers, the obtained FeOCN pressure sensor demonstrates a wide working range (0–4.9 kPa) and a high sensitivity of 0.545 kPa^{-1} as well as an ultralow detection limit of 6 Pa. Additionally, the pressure sensor exhibits, rapid response time, good stability, high hydrophobicity, and excellent flexibility. These merits endow the pressure sensor with the ability to precisely detect wrist pulse, phonation, breathing, and finger bending in real-time.

2. Materials and methods

2.1. Materials

Polyacrylonitrile (PAN, $M_W = 150\,000$) powder was purchased from Sigma-Aldrich, Co., Ltd. N,N-Dimethylmethanamide (DMF, 99.8%) was purchased from Aladdin Chemical Co., Ltd. Ferric chloride ($FeCl_3$, 97%) was purchased from Beijing Chemical Works. And all chemicals were used as received.

2.2. Preparation of 3D electrospun carbon nanofibers and FeOCN pressure sensor

1.2 g PAN powder was dissolved in 8.8 g DMF solvent, the mixture was magnetic stirred at 60 °C for 4 h until complete dissolution. Then, 0.4 g $FeCl_3$ was dissolved in the obtained polymer solution with magnetic stirring at 60 °C for 18 h. Afterward, the prepared precursor solution was injected into a 5 ml syringe connected to a metal needle. The electrospinning procedure was carried out using a 20 kV voltage, with a nozzle-to-collector distance of 18 cm, the feeding rate was controlled at 0.5 ml h^{-1}. The precursor 3D nanofibers were collected on the aluminium foil of an autonomous rotating drum at a fixed rotation speed of 120 rpm. After electrospinning, a thick of precursor 3D nanofibers was obtained, and then dried at 60 °C for 5 h.

The oxidative stabilization was implemented in a tube furnace in an air atmosphere, the precursor 3D nanofibers were heated from room temperature to 210 °C for 2 h with a heating rate of 5 °C min^{-1}, and then cooled to room temperature. Subsequently, the oxidative stabilized 3D nanofibers were carbonized by heating tube furnace from room temperature to 800 °C at 5 °C min^{-1} in the nitrogen atmosphere and kept at 800 °C for 2 h. Finally, two pieces of copper foil electrodes were

glued with conductive silver past at the upper and lower surfaces of the 3D electrospun carbon nanofibers, and the dimension of the FeOCN pressure sensor fabricated is around $23.4 \times 8.54 \times 3$ mm^3.

2.3. Characterization

The morphologies of the electrospun carbon nanofibers and their corresponding element mapping were imaged by a scanning electron microscopy (SEM, SHIMADZUX-550) equipped with an energy-dispersive X-ray spectroscope (SEDX-500, Shimadzu). Raman spectra were recorded using a laser with a wavelength of 532 nm (Jobin-Yvon Horiba T64000 Raman triple grating spectrometer). Water contact angles (WCAs) of the electrospun carbon nanofibers were tested with an optical contact angle & interface tension meter (SL200KS). To investigate piezoresistive performances of the FeOCN pressure sensor, compression tests were measured by a STD100 microcomputer-controlled electronic universal testing machine (RicKs Measurement and Control Co., Ltd.). The responsive electrical signals of the FeOCN pressure sensor were measured by a Keysight B2902A Precision Source/Measure Unit (KEYSIGHT B2902A).

3. Results and discussion

Fig. 1a illustrates the fabrication process of FeOCN pressure sensor. Firstly, the 3D nanofibers were directly prepared by electrospinning. The as-prepared 3D nanofibers were dried and oxidative stabilized in air condition. Subsequently, the oxidative stabilized 3D nanofibers were carbonized through a high temperature treatment in the nitrogen atmosphere. Finally, the FeOCN pressure sensor is obtained by using two copper foil glued at both sides of the 3D electrospun carbon nanofibers. Fig. 1b and c shows SEM images of the 3D electrospun carbon nanofibers. The average diameter of the carbonized nanofibers is around 763 nm. From the SEM image of Fig. 1b, it could be observed that carbon nanofibers are fluffy, uniform, porous and interweave 3D networks. According to the high-magnification SEM image of Fig. 1c, it is shown that both in-focus carbon nanofibers and relative blurry, out-of-focus carbon nanofibers, which is proof the 3D structure of the carbon nanofibers network. When pressed and bent, the carbonized 3D nanofibers network exhibits excellent flexibility (Video S1†). Meanwhile, the surfaces of the 3D carbon nanofibers are rough and wrinkled. Fig. 1d shows the Raman spectra of the FeOCN. An intensive absorption at ≈ 1596 cm^{-1} (G band) demonstrates the existence of ordered graphitic structure and absorption at ≈ 1365 cm^{-1} (D band) is attributed to the disorders or defects of carbon.[31] The intensity ratio of D band to G band (I_D/I_G) is around 1.14, indicating that FeOCN is partially graphitized. Graphitization will help increase the conductivity of the FeOCN.[32] With the increase in the conductivity of the 3D carbon nanofibers network, it will benefit increase the sensitivity of the FeOCN pressure sensor.[33] After a series of heat treatments, Fe^{3+} ions were oxidized to Fe_3O_4. The C, Fe, O are homogeneously distributed on the 3D carbon nanofibers surface as shown in the
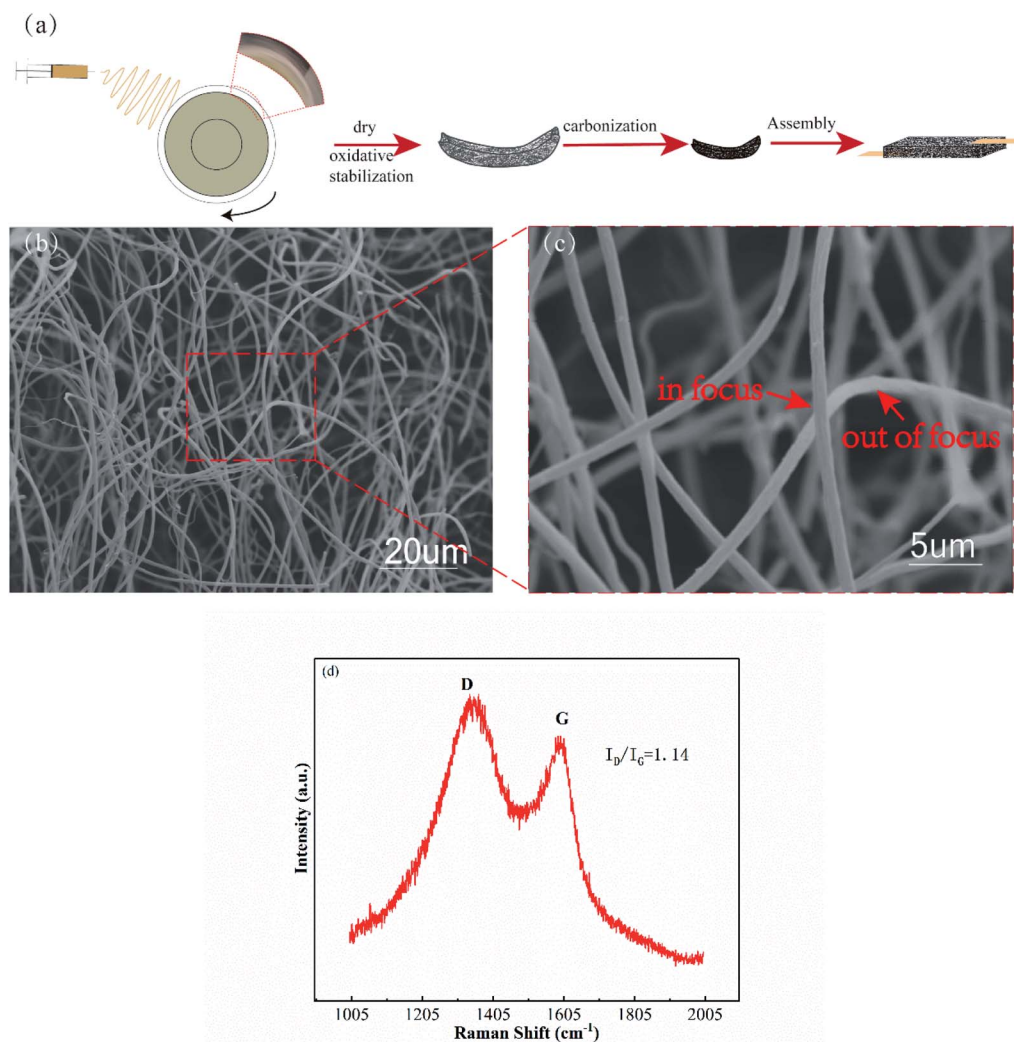
Fig. 1 (a) Schematic illustration showing the fabrication process of FeOCN pressure sensor. (b) Low and (c) high-magnification SEM images of the 3D carbon nanofibers. (d) Raman spectra of the FeOCN under 800 °C.

element mapping images of Fig. S1.† The wetting behavior of 3D carbon nanofibers was tested by the method of drop shape analysis (DSA). As shown in Fig. S2,† the water contact angle was measured between a drop of water and the surface of the 3D carbon nanofibers surface. And the water contact angle is 130.326°, indicating the 3D carbon nanofibers was high hydrophobicity. This hydrophobicity is caused by the additions of PAN[34] and $FeCl_3$,[35] as well as the rough and wrinkled surface of carbon nanofibers.[35,36] Besides, the hydrophobic properties will contribute to the waterproof properties of the FeOCN pressure sensor, which is imperative for the practical applications of them.[37,38]

In this work, the electrospun nanofibers could self-assemble into the 3D nanofibers network structure. Sun Bin, *et al.* in a published study revealed the necessary conditions for the formation of a 3D fiber structure, namely needs a conductive collector plate to facilitate the charge transfer of the coming fibers.[2,39] Meanwhile, under the influence of an applied strong electrostatic field, the top of the electrospun nanofibers will be
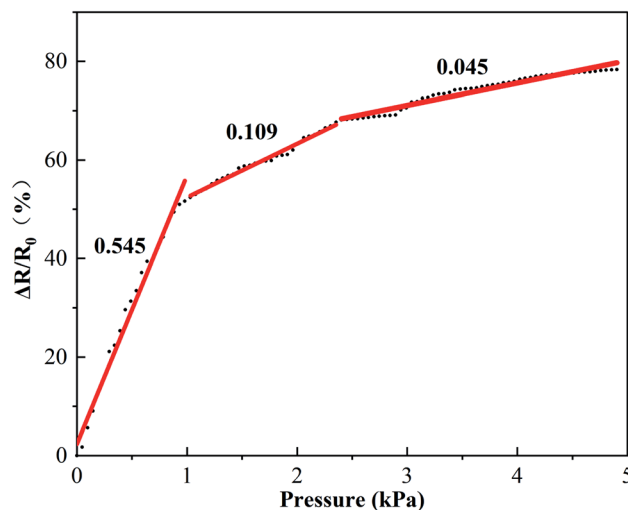

Fig. 2 Relative resistance variation ratios as a function of pressure for the FeOCN pressure sensor.

Table 1 Comparison of pressure highest sensitivity, work range, and other versatile properties of various 3D porous materials

Materials	Highest sensitivity (kPa^{-1})	Work range (kPa)	Hydrophobicity	Reference
Carbon nanofiber networks	1.41 (0–0.25 kPa)	0–2.5	√	25
Copper nanowires/reduced graphene oxide/melamine foam	0.088 (1.5–10 kPa)	0–18	—	45
CNTs/GO@PDMS	0.31 (0.05–3.8 kPa)	0.05–6.3	√	46
rGO/PI foam	0.18 (0–1.5 kPa)	0–6.5	—	47
RGO-PU sponge	0.26 (0–2 kPa)	0–10	—	48
FeOCN	0.545 (0–1 kPa)	0–4.9	√	This work

negatively charged and attracted by the metal needle, which will facilitate the continued self-assembly of the nanofibers.[39] As we know, not all polymer solutions can be directly electrospun into a 3D self-assembly structure. And electrospinning solution is the most critical factor that can have a significant impact on the formation of 3D nanofibers network structure.[21] The addition of Fe^{3+} in the electrospinning solution is the key to building 3D nanofibers network structure.[2] Under the action of electrostatic the Fe^{3+} will be easily magnetized or polarized, this will decrease the fiber diameter and lead to a loose and fluffy 3D nanofibers network.[39] Besides, an appropriate choice of solvent will also benefit the fiber to quickly solidify, so it has enough strength to support subsequent fibers accumulation. As a common organic solvent, DMF has been widely used in 3D electrospinning.[22,25,40,41] Compared with other solvents, such as dimethylsulfoxide (DMSO), N-methylpyrrolidone (NMP), DMF has the advantage of rapid evaporation in electrospinning.[42] So the rapid evaporation of the DMF will help maintain the 3D nanofibers network structure. Besides, the influence of the distance from the nozzle-to-collector on the formation of the 3D nanofibers network is also considered. Kirecci Ali, et al. found that as the distance increases, the diameter of the fiber will first decrease and then increase, where the minimum fiber diameter is obtained when the distance is 15 cm.[43] In another work, reported by Jalili R. et al. they found that when the receiving distance is less than 15 cm, the solvent is not completely evaporation.[44] The two works mentioned above are related to the use of PAN/DMF solution for electrospinning. It can be seen that appropriately increasing the distance from the nozzle to the collector is beneficial to the solidification of the fiber and can effectively control the diameter of the fiber. Therefore, in this work, an appropriate distance was selected, that is, the distance from the nozzle to the collector is 18 cm. It can ensure that the collected fibers are almost completely solidified when in contact with the collector, which will help the construction of the 3D nanofibers network.

Fig. 2 shows the relative resistance variation ratios ($\Delta R/R_0 = (R_0 - R)$, where R_0 and R denote the resistance without and with load pressure, respectively) of the FeOCN pressure sensor with the applying of different pressure. It showed that the relative resistance variation ratios of the FeOCN pressure sensor was gradually increased with the increase of the load pressure, which could be divided into three regions: low pressure range (0–1 kPa), middle pressure range (1–2.4 kPa), high pressure

range (2.4–4.9 kPa). The sensitivity (S) of the FeOCN pressure sensor is defined as $S = \delta(\Delta R/R_0)/\delta P$, where ΔR and P denote the change in resistance and the applied pressure, respectively. The S of the FeOCN pressure sensor in the pressure range of 0–1 kPa, 1–2.4 kPa and 2.4–4.9 kPa calculated is 0.545 kPa^{-1}, 0.109 kPa^{-1} and 0.045 kPa^{-1}, respectively. In the low pressure regime (0–1 kPa), the FeOCN pressure sensor shows a high sensitivity of 0.545 kPa^{-1}, which is around 5 and 12 times larger than the middle and high pressure range. Table 1 shows the comparison of pressure highest sensitivity, work range, and other versatile properties of various 3D porous materials. Obviously, the FeOCN pressure sensor shows both a relatively high sensitivity as well as a wide pressure detection range.

The working mechanism of the FeOCN pressure sensor could be explained by the contact resistance change between the tangled carbon nanofibers induced by the load pressure.[4,9,25] And the increased contact sites will cause more conductive paths. Under a small pressure, the lower the density of the contact sites, the higher the relative increase of the contact sites, which will lead to higher sensitivity. As the pressure continued to increase, the density of contact sites will decrease accordingly and will get a relatively low relative increase in contact sites, which will lead to lower sensitivity. The schematic evolution of the FeOCN pressure sensor sensing models is shown in Fig. S3.†

The as-fabricated FeOCN pressure sensor demonstrates an excellent sensing performance. As shown in Fig. 3a, the current–voltage curves of the FeOCN pressure sensor under different pressure show good linear ohmic characteristics, which indicate the FeOCN pressure sensor exhibits a stable response to static pressure. Meanwhile, the slope of the current–voltage curves increases significantly with the pressure increase from 50 to 2500 Pa, due to the corresponding increase of the conductivity. To investigate the detection limit of the FeOCN sensor, a tiny weight (0.1218 g) was cyclically loaded and unloaded on the sensor (23.4 mm × 8.54 mm). And Fig. 3b illustrates the relative resistance variation ratios response of the FeOCN pressure sensor during the loading and unloading of a small pressure less than 6 Pa. The low detection limit enables the sensor to detect human pulses. To evaluate the reliability and repeatability of the pressure sensor, various compression tests were performed. As illustrated in Fig. 3c, when the sensor under compressive loading–unloading cycles with different applied pressure values of 50, 60, 70, 120, and 2500 Pa, the relative
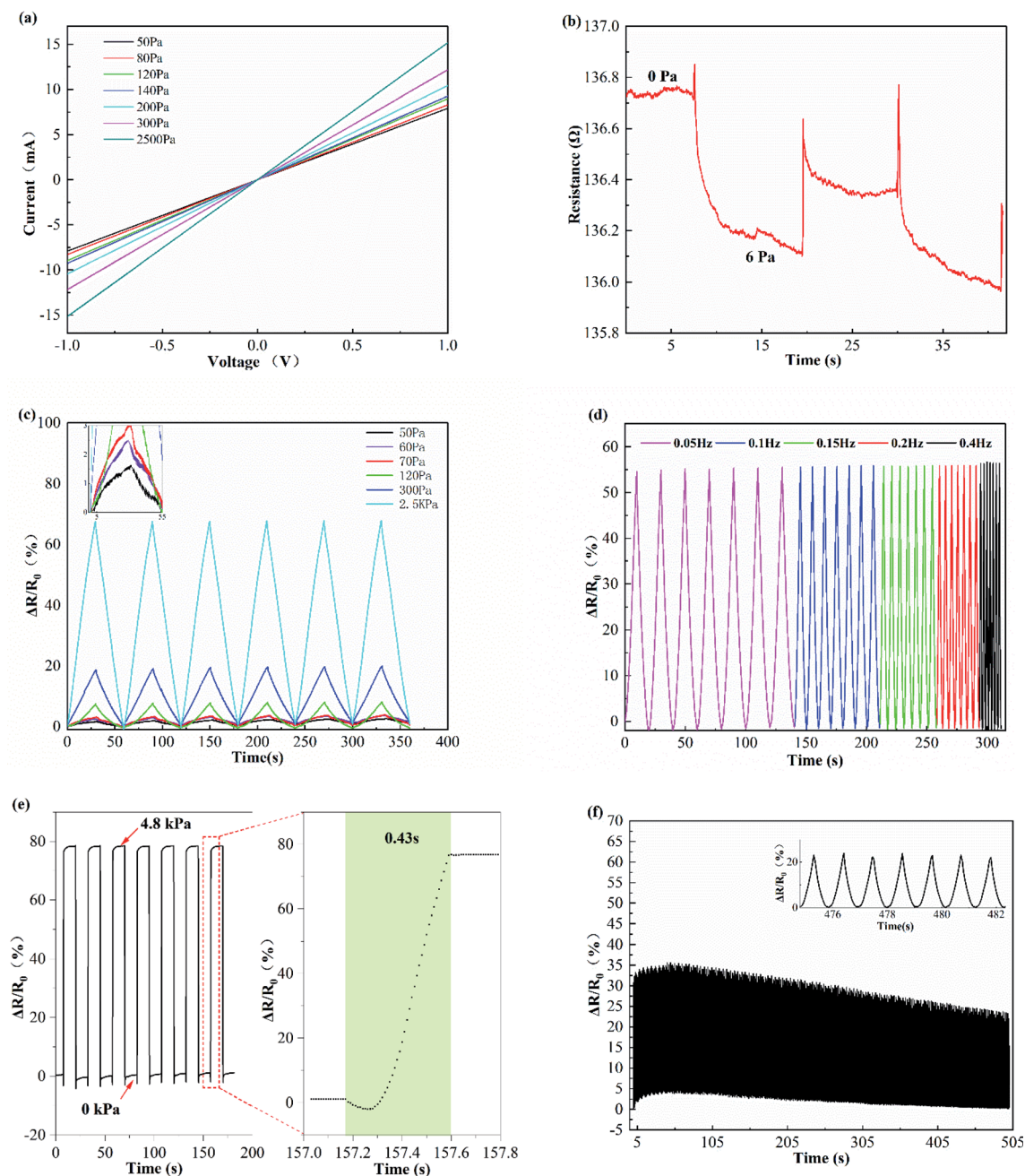
Fig. 3 (a) Current–voltage curves of the FeOCN pressure sensor under different load pressures in the range of 50–2500 Pa. (b) The detection limit of the FeOCN pressure sensor, which displays the relative resistance variation ratios upon loading a small pressure less than 6 Pa. (c) Multiple cycles tests of repeated loading and unloading pressure at 50, 60, 70, 120, 300, 2500 Pa, respectively. The inset shows the magnified loading and unloading pressure curves at 50, 60, 70 Pa. (d) Relative resistance variation response of the FeOCN pressure sensor at varying frequencies. (e) Pressure response at high frequency and enlarged view on the right shows the response time of about 0.43 s. (f) The durability test of the FeOCN pressure sensor over 500 loading–unloading cycles at an applied pressure of 0.5 kPa and a frequency of 1 Hz. The inset shows the magnified curves of 7 cycles after 475 cycles.

resistance variation ratios increased monotonically with the increase of applied pressures, and the response signals of the sensor were basically identical to the given pressure. In general, the FeOCN pressure has a good response to different applied pressures. Considering that loading frequency dependence is one of the important characteristics that need to be considered for a sensor. The response of the FeOCN pressure sensor at

various compression frequency strain rates from 0.05 to 0.4 Hz is investigated. As shown in Fig. 3d, the relative resistance variation response signals exhibit a similar response. Meanwhile, the magnitude of the relative resistance variation peak is almost the same. The FeOCN pressure sensor showed highly steady and almost no dependence on the loading rate, suggesting that the FeOCN pressure sensor is sensitive in a wide
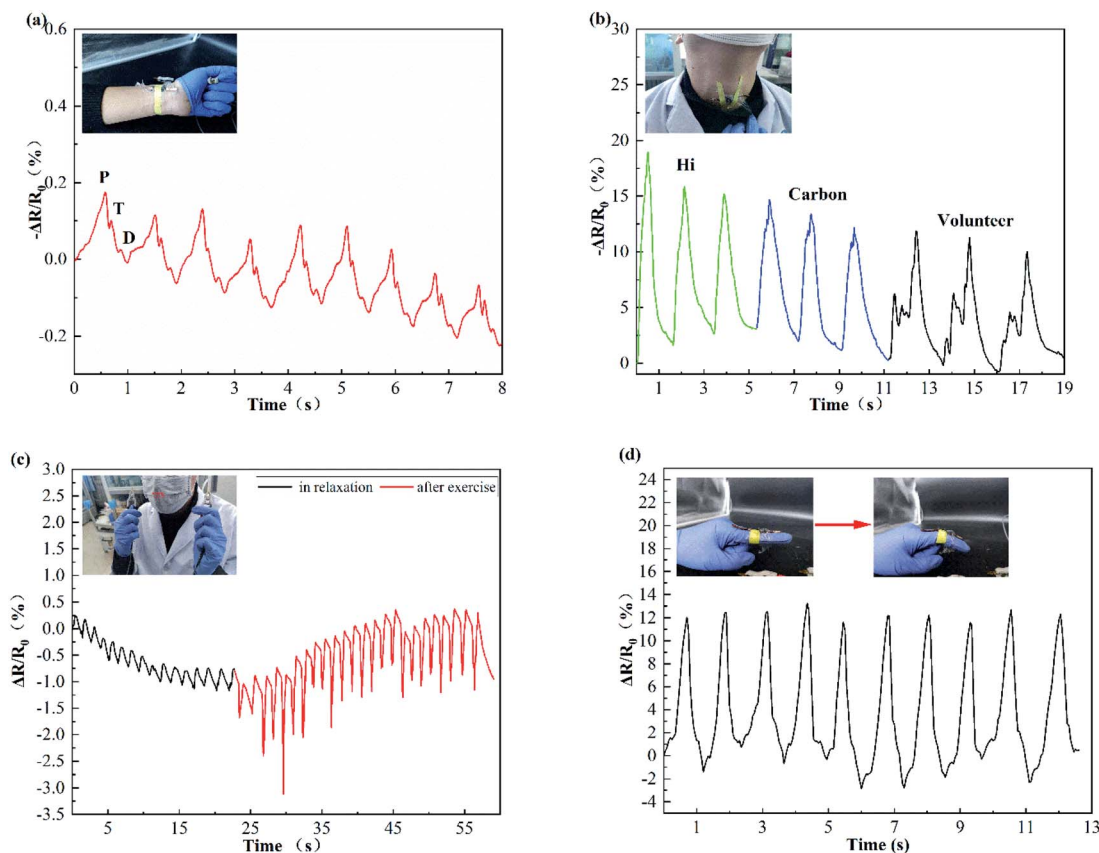
Fig. 4 (a) The response signals of the FeOCN pressure to various human motions: (a) wrist pulse, (b) phonation, (c) breathing and (d) finger bending.

range of frequency and has excellent robustness. In order to investigate the response time of the FeOCN pressure sensor, dynamic pressure inputs have been applied. As shown in Fig. 3e, the pressure sensor showed an immediate response to loading/unloading of 4.8 kPa, with a response time of about 0.43 s. The long response time may be caused by the hysteresis effect of the FeOCN pressure sensor during loading/unloading pressure. Moreover, in order to evaluate the reproducibility and durability of the FeOCN pressure sensor, as can be seen from Fig. 3f, the pressure response over 500 loading–unloading cycles at an applied pressure of 0.5 kPa and a frequency of 1 Hz was recorded. The FeOCN pressure sensor showed excellent reproducibility and durability with negligible changes in 500 times presses. As shown in the enlarged inset in Fig. 3f, the output curve remains nearly identical sharp resistance amplitude after each loading and unloading cycles, which indicates that the sensor has a long working life and high stability. The above results approve that the FeOCN pressure sensor features high sensitivity, rapid response, and excellent repeatability, also, the pressure sensor does not require sophisticated microstructures design or expensive conductive materials.

Based on their superior performance, the FeOCN pressure sensor can be potentially employed to detect various human motions in real-time, such as wrist pulse, phonation, breathing, and finger bending. Pulse rate is one of the vital signs of human life and pulse can also be used to diagnose in Traditional

Chinese Medicine.[49] So accurate collection of pulse signals is helpful to assess the health state of the human body. Fig. 4a shows a FeOCN pressure sensor fixed on the wrist to monitor the pulse in real-time. And pulse shapes are regular and repeatable. In particular, three typical characteristic peaks of wrist pulses were collected, which correspond to percussion wave (P-wave), tidal wave (T-wave), and diastolic wave (D-wave), respectively. So the FeOCN pressure sensor possesses a potential application in wearable electrical skin. As shown in Fig. 4b, the FeOCN pressure sensor was attached to the throat to monitor the phonation. Characteristic waves of some words including the monosyllabic word "hi", a dissyllabic word "carbon", and a polysyllabic word "volunteer" can be recognized. At the same time, the response signal curves of each word can be easily distinguished by analysing the shape of the response signal curves, indicating the sensor can be potential employed in human voice recognition. Fig. 4c shows that the FeOCN pressure sensor fixed in the breathing position inside the mask, the real-time breath pulses of a volunteer in relaxation and after exercise were recorded. Two pulse patterns are easy to identify after exercise and in relaxation, and both of them show good repeatability. Compared to a relaxed state, the response amplitude after exercise increased more obviously. The results reveal the promising possibility of respiratory rate detection. As shown in Fig. 4d, the FeOCN pressure sensor was mounted onto the index finger to identify the bending

deformation at different angles, the response signal under different bending angles can be easily identified, which provides a promising application for identifying the bending angle of the finger. The above results indicate that the FeOCN pressure sensor has great potential for detecting various human motions.

4. Conclusions

In summary, a flexible FeOCN pressure sensor with high sensitivity at a wide working range has been successfully fabricated using 3D electrospinning and further carbonization methods. Importantly, the interweaved 3D carbon nanofibers network structure can be directly obtained by simple electrospinning followed by thermal treatment and does not require sophisticated microstructures design or expensive conductive materials. The formation mechanism of the self-assembly 3D nanofibers network structure has been systematically explored, in which Fe^{3+} as an ion source is the key to building 3D nanofibers network structure. The working mechanism of the FeOCN pressure sensor could be explained by the contact resistance change between the tangled carbon nanofibers induced by the load pressure. Furthermore, the as-fabricated FeOCN pressure sensor demonstrates a wide working range (0–4.9 kPa) and high sensitivity of 0.545 kPa^{-1} as well as an ultralow detection limit of 6 Pa. Meanwhile, the pressure sensor showed some good features, such as rapid response time, good stability, high hydrophobicity, and excellent flexibility. Finally, based on the superior performance of the FeOCN pressure sensor, human motions including wrist pulse, phonation, breathing, and finger bending were successfully monitored, indicating that the FeOCN pressure sensor may have a promising prospect for real-time healthcare monitoring.

Conflicts of interest

There are no conflicts to declare.

Acknowledgements

Notes and references

1 Y. Ding, T. Xu, O. Onyilagha, H. Fong and Z. Zhu, ACS Appl. Mater. Interfaces, 2019, 11, 6685–6704.
2 O. Y. Kweon, S. J. Lee and J. H. Oh, NPG Asia Mater., 2018, 10, 540–551.
3 Z. Zhou, Y. Li, J. Cheng, S. Chen, R. Hu, X. Yan, X. Liao, C. Xu, J. Yu and L. Li, J. Mater. Chem. C, 2018, 6, 13120–13127.
4 Q. Wang, M. Jian, C. Wang and Y. Zhang, Adv. Funct. Mater., 2017, 27, 1605657.
5 K. Ke, M. McMaster, W. Christopherson, K. D. Singer and I. Manas-Zloczower, Composites, Part A, 2019, 126, 105614.
6 J. Liu, B. Yang, L. Lu, X. Wang, X. Li, X. Chen and J. Liu, Sens. Actuators, A, 2020, 303, 111796.
7 Z. Li, M. Zhu, J. Shen, Q. Qiu, J. Yu and B. Ding, Adv. Funct. Mater., 2020, 30, 1908411.
8 A. Fiorillo, C. Critello and S. Pullano, Sens. Actuators, A, 2018, 281, 156–175.
9 Z. Han, H. Li, J. Xiao, H. Song, B. Li, S. Cai, Y. Chen, Y. Ma and X. Feng, ACS Appl. Mater. Interfaces, 2019, 11, 33370–33379.
10 Z. Chen, Z. Wang, X. Li, Y. Lin, N. Luo, M. Long, N. Zhao and J.-B. Xu, ACS Nano, 2017, 11, 4507–4513.
11 D. Sengupta, Y. Pei and A. G. P. Kottapalli, ACS Appl. Mater. Interfaces, 2019, 11, 35201–35211.
12 S. M. Doshi and E. T. Thostenson, ACS Sens., 2018, 3, 1276–1282.
13 W. Zhong, C. Liu, Q. Liu, L. Piao, H. Jiang, W. Wang, K. Liu, M. Li, G. Sun and D. Wang, ACS Appl. Mater. Interfaces, 2018, 10, 42706–42714.
14 B. Zhu, Y. Ling, L. W. Yap, M. Yang, F. Lin, S. Gong, Y. Wang, T. An, Y. Zhao and W. Cheng, ACS Appl. Mater. Interfaces, 2019, 11, 29014–29021.
15 M. Weng, L. Sun, S. Qu and L. Chen, Extreme Mech. Lett., 2020, 100714.
16 X. Jiang, Z. Ren, Y. Fu, Y. Liu, R. Zou, G. Ji, H. Ning, Y. Li, J. Wen and H. J. Qi, ACS Appl. Mater. Interfaces, 2019, 11, 37051–37059.
17 Y. Ma, M. Yu, J. Liu, X. Li and S. Li, ACS Appl. Mater. Interfaces, 2017, 9, 27127–27134.
18 Y. Si, X. Wang, C. Yan, L. Yang, J. Yu and B. Ding, Adv. Mater., 2016, 28, 9512–9518.
19 Y. Hu, H. Zhuo, Z. Chen, K. Wu, Q. Luo, Q. Liu, S. Jing, C. Liu, L. Zhong and R. Sun, ACS Appl. Mater. Interfaces, 2018, 10, 40641–40650.
20 Y. Wan, N. Qin, Y. Wang, Q. Zhao, Q. Wang, P. Yuan, Q. Wen, H. Wei, X. Zhang and N. Ma, Chem. Eng. J., 2020, 383, 123103.
21 H.-Y. Mi, X. Jing, B. N. Napiwocki, Z.-T. Li, L.-S. Turng and H.-X. Huang, Chem. Eng. J., 2018, 331, 652–662.
22 M. M. Li and Y. Z. Long, 2011.
23 B. Sun, Y. Long, H. Zhang, M. Li, J. Duvail, X. Jiang and H. Yin, Prog. Polym. Sci., 2014, 39, 862–890.
24 Y. Chen, M. Shafiq, M. Liu, Y. Morsi and X. Mo, Bioact. Mater., 2020, 5, 963–979.
25 Z. Han, Z. Cheng, Y. Chen, B. Li, Z. Liang, H. Li, Y. Ma and X. Feng, Nanoscale, 2019, 11, 5942–5950.
26 J. C. Yang, J.-O. Kim, J. Oh, S. Y. Kwon, J. Y. Sim, D. W. Kim, H. B. Choi and S. Park, ACS Appl. Mater. Interfaces, 2019, 11, 19472–19480.
27 J. Oh, J. O. Kim, Y. Kim, H. B. Choi, J. C. Yang, S. Lee, M. Pyatykh, J. Kim, J. Y. Sim and S. Park, Small, 2019, 15, 1901744.

28 B. Feng, G. Zou, W. Wang, M. Dong, Y. Xiao, H. Ren, X. Zhao, G. Zhao, A. Wu and H. Zhu, *Nano Energy*, 2020, 104847.

29 Y. Luo, J. Shao, S. Chen, X. Chen, H. Tian, X. Li, L. Wang, D. Wang and B. Lu, *ACS Appl. Mater. Interfaces*, 2019, **11**, 17796–17803.

30 R. Chen, Y. Hu, Z. Shen, P. Pan, X. He, K. Wu, X. Zhang and Z. Cheng, *J. Mater. Chem. A*, 2017, **5**, 12914–12921.

31 Q. Wang, M. Jian, Z. Chunya and Z. Yingying, *Adv. Funct. Mater.*, 2017, **27**, 1605657.

32 Z. Zhang, W. Yang, L. Cheng, W. Cao, M. Sain, J. Tan, A. Wang and H. Jia, Carbon Fibers with High Electrical Conductivity: Laser Irradiation of Mesophase Pitch Filaments Obtains High Graphitization Degree, *ACS Sustainable Chem. Eng.*, 2020, **8**, 17629–17638.

33 Z. Zhang, W. Yang, L. Cheng, W. Cao and H. Jia, *ACS Sustainable Chem. Eng.*, 2020, **8**, 17629–17638.

34 I. M. Alarifi, A. Alharbi, W. S. Khan, A. Swindle and R. Asmatulu, *Materials*, 2015, **8**, 7017–7031.

35 Y. Ding, W. Xu, Y. Yu, H. Hou and Z. Zhu, *ACS Appl. Mater. Interfaces*, 2018, **10**, 6652–6660.

36 C. W. Schultz, C. L. Ng and H.-Z. Yu, *ACS Appl. Mater. Interfaces*, 2019, **12**, 3161–3170.

37 S. Sun, Y. Liu, X. Chang, Y. Jiang, D. Wang, C. Tang, S. He, M. Wang, L. Guo and Y. Gao, *J. Mater. Chem. C*, 2020, **8**(6), 2074–2085.

38 H. Liu, Q. Li, Y. Bu, N. Zhang and C. Shen, *Nano Energy*, 2019, 104143.

39 B. Sun, Y.-Z. Long, F. Yu, M.-M. Li, H.-D. Zhang, W.-J. Li and T.-X. Xu, *Nanoscale*, 2012, **4**, 2134–2137.

40 M. H. Tai, B. Y. L. Tan, J. Juay, D. D. Sun and J. O. Leckie, *Chem.–Eur. J.*, 2015, **21**, 5395–5402.

41 L. Cao, Y. Si, X. Yin, J. Yu and B. Ding, *ACS Appl. Mater. Interfaces*, 2019, **11**, 35333–35342.

42 N. Ucar, N. Kizildag, A. Onen, I. Karacan and O. Eren, *Fibers Polym.*, 2015, **16**, 2223–2236.

43 A. Kirecci, Ü. Özkoç and H. İ. İçoğlu, *J. Appl. Polym. Sci.*, 2012, **124**, 4961–4968.

44 R. Jalili, S. A. A. Hosseini and M. Morshed, *J. Kerbala University*, 2005, 1074–1081.

45 Y. Xiong, Y. Zhu, X. Liu, P. Zhu and C. P. Wong, *Mater. Today Commun.*, 2020, **24**, 100970.

46 C. Mu, Y. Song, W. Huang, A. Ran, R. Sun, W. Xie and H. Zhang, *Adv. Funct. Mater.*, 2018, **28**, 1707503.

47 Y. Qin, Q. Peng, Y. Ding, Z. Lin, C. Wang, Y. Li, F. Xu, J. Li, Y. Yuan, X. He and Y. Li, *ACS Nano*, 2015, **9**, 8933.

48 H. B. Yao, J. Ge, C. F. Wang, X. Wang, W. Hu, Z. J. Zheng, Y. Ni and S. H. Yu, *Adv. Mater.*, 2013, **25**, 6692–6698.

49 T. Yang, X. Jiang, Y. Zhong, X. Zhao, S. Lin, J. Li, X. Li, J. Xu, Z. Li and H. Zhu, *ACS Sens.*, 2017, **2**, 967–974.